International Journal of Thermal Sciences 129 (2018) 94–105

Contents lists available at ScienceDirect

International Journal of Thermal Sciences

journal homepage: www.elsevier.com/locate/ijts

An experimental study of natural convection in a distribution transformer slice model

Paola A. Córdoba*[,1], Nicolás Silin[2], Darío Osorio[3], Enzo Dari[1]

Instituto Balseiro, Universidad Nacional de Cuyo, Centro Atómico Bariloche-CNEA, Av. Bustillo, 9500, S.C. de Bariloche, Río Negro, Argentina

ARTICLE INFO

Keywords:
ONAN distribution transformer
Particle Image Velocimetry (PIV)
Natural convection

ABSTRACT

The aim of this work is to obtain experimental information on the thermal and fluid dynamics of a distribution transformer. The transformer of interest is of the oil natural – air natural type and our interest is centered in the natural circulation that is produced in the oil volume. An experimental device was built to simulate a representative slice of the transformer and a purpose built PIV setup was used to obtain the flow velocity field. The device overall dimensions and the refrigerating oil are the same as those of commercial transformers of 1000 KVA (Tubos Trans Electric S.A. 1000 KVA Standard Distribution Transformer) Natural circulation is produced by a heating element simulating the heat produced by copper losses in the transformer. A double glass window allows visual access for flow visualization and PIV capture. The slice comprises two fins and the air side is bounded by two isolating boards, forming three air channels. Two reference powers were tested for the experiment: The power corresponding to design operating conditions and a lower power to observe the sensibility to power variations. The result reported in this work shows features of the flow pattern that give important information on the sort of turbulent mixing to be expected. The transient evolution was measured and the thermal characteristic time of the system was estimated. It was found that the convection during the start-up transient is significantly stronger than during steady state operation.

1. Introduction

The main motivation of this work is to measure experimentally the oil flow pattern and the heat transfer in an ONAN (Oil Natural Air Natural) type power transformer. This type of transformers are oil filled. This oil acts both as electrical insulator and as coolant fluid, maintaining the temperature of electrical components within acceptable limits. Transformers produce heat in the ferromagnetic core and in the coils due to unavoidable power losses. The oil is heated by the core and the coils and circulates to the hollow fins, where it is cooled down. The fins provide an exchange surface with the air and heat is transferred, again by natural convection to the atmosphere, therefore the ONAN denomination. In the design of interest, fins are integral part of the walls being manufactured by folding a metal sheet. The resulting flexibility of the walls allows to compensate the volume changes of the oil without an expansion tank.

There are both, country specific regulations (In Argentina we have the [1]) and international standards [2,3] that define the allowable operation conditions for these devices. These regulations give mathematical models for the calculation of operating temperatures in the transformer, in particular the temperature of the hottest spot of the winding. The [2] also suggest a series of working temperature boundaries to avoid premature degradation of the oil or the transformer materials. In spite of these regulations it is still up to the manufacturer to achieve a design that satisfies these limits while minimizing the size and cost of the transformer. This is a rather challenging task that normally involves trial and error and ends up with varying degrees of over dimensioning.

These thermohydraulic devices have been widely studied in order to improve their efficiency and lifespan. One of the aspects of greatest interest is the point of maximum temperature or the hottest-spot winding temperature, due to the fact that it is the principal factor in determining the life time due to loading. Researchers use different methods to determine the hot spot temperature [4]: proposed a numerical method to obtain the temperature distribution in the power transformer windings in a transformer with non-directed oil forced (NDOF) and directed oil forced cooling. They took into account the winding structure in contrast to the calculation procedure given in the

* Corresponding author.
E-mail addresses: paolaco@cab.cnea.gov.ar (P.A. Córdoba), silin@cab.cnea.gov.ar (N. Silin), osorio@cab.cnea.gov.ar (D. Osorio), darie@cab.cnea.gov.ar (E. Dari).
[1] Departamento de Mecánica Computacional, Centro Atómico Bariloche, CNEA-Conicet, Av. Bustillo 9500, Argentina.
[2] Departamento de Materiales Nucleares, Centro Atómico Bariloche, CNEA-Conicet, Av. Bustillo 9500, Argentina.
[3] Laboratorio de Termohidráulica, Centro Atómico Bariloche, CNEA, Av. Bustillo 9500, Argentina.

https://doi.org/10.1016/j.ijthermalsci.2018.02.029
Received 21 December 2016; Received in revised form 21 February 2018; Accepted 26 February 2018
Available online 08 March 2018
1290-0729/

international Standards ([2]) which contains simplified calculation methods [5]. presented a thermal modeling based on the thermal-electrical analogy and heat transfer theory to predict the top-oil and hot-spot temperature in ONAN cooled transformers. In posterior works [6,7], took into account the oil viscosity changes and power loss variation with temperature in their improved thermal modeling. The life span of the transformer is also strongly influenced by the condition of the solid insulation (paper and pressboard). At higher temperatures, the solid insulation can suffer deterioration reducing its life span [2]. A discussion of this topic can be found in the work of [8]. The authors also suggest a method for life cycle prediction based on measurements of insulating resistance at several temperatures. It is also known that the dielectric oil, can degrade over time to the point that the device can not withstand severe events such as overvoltage or short circuit [9]. Hajidavalloo et al. in Ref. [10] added an experimental component analyzing the temperature rise in a ONAN type transformer by effects of radiation. Their model predicts the temperature values measured in their experimental study. They also evaluated the use of a protective awning to extend the life time of the device.

The ONAN heat transfer scheme has proven reliable and cost effective. Yet the assessment of these schemes require to tackle the combination of two natural convection systems, and a complex geometry involving different length scales, and the variable properties of the fluids involved. These characteristics make both, experimental and numerical assessments, rather challenging. Also, this heat transfer scheme involves different phenomena that have been studied separately due to their engineering interest. The natural convection problem has been widely studied for its engineering applications in solar collectors [11] and research reactors [12], among others. For these studies the geometries are typically simplified cubic or prismatic cavities with fixed boundary conditions. We can mention the studies by Refs. [13–15] on the natural convection flow in a wide range of Rayleigh numbers, or the works of [16–19] on the influence of the temperature dependence of the fluid properties on the flow patterns. The transition to turbulence is a topic that has been studied for natural convection problems with constant properties of the fluid [20,21], being an unexplored topic for the case of variable properties. When determining the flow field and the temperatures in an ONAN transformer, these phenomena have to be accounted for to produce a realistic result, making both experimental and numerical assessment quite challenging. The experimental studies regarding these devices are limited. Most of the works available in the literature, only involve temperature measurements in transformer prototypes equipped with temperature sensors at some points of interest within the device [5,10,22–25]. Typically, such thermo probes are thermocouples or optical fiber based temperature sensors [25]. All experimental works mentioned above have been used to verify thermal models. Therefore, the experimental measurement of the flow field in these devices is still a rather unexplored area.

Natural convection in oil cooled transformers has been widely studied from the computational point of view. The CFD approach allows not only to predict the hot spot temperature but also the temperature distribution and the flow pattern. The knowledge of the fluid field inside transformer can then be used to optimize its cooling. [26–28], among others, studied the thermal distribution and flow pattern in a disc-type power transformer by CFD modeling of the cooling channels in the winding. Regarding ONAN type transformers, and due to the complexity of the problem, modeling all the details of the transformer structure is still computationally expensive. Thus, depending on the researcher, several geometric simplifications are used, [24,29–31]. [30], built two separated models, one for the solid active parts of the transformer, i.e. winding and core, and one for the oil tank. Then they coupled the results of the thermal solver with the CFD solver in an iterative process obtaining the temperature distribution. They point out that an experimental validation of their oil local velocity results is quite difficult. [24], and [31] presented a simplified mathematical model of the oil flow and heat transfer inside an ONAN transformer. In both models, the oil flow domain is reduced to a slice of the complete transformer, with some differences in the solution method and in the simplifications considered. The models predict a stratified temperature distribution and a notable rising oil plume generated at the outlet of the winding channels [24]. used a turbulent model, justified by their high Rayleigh number estimations, however the thermal models used to predict the hot-spot temperature of [6] assume laminar flow inside the transformer. The nature of the flow inside these devices is not clear yet due to the lack of experimental studies regarding the flow pattern. This flow could as well be laminar, fluctuating or turbulent.

In this work we perform measurements on an experimental device that simulates a representative slice of an ONAN distribution transformer. There have been several considerations to make this slice a good representation of the real transformer. The device uses a commercial transformer oil and the overall dimensions are the same as those of a commercial transformer of 1000 KVA (Tubos Trans Electric S.A. 1000 KVA Standard Distribution Transformer). The experimental device is composed of a heating element simulating the heating by copper losses in the transformer. A double glass window allows visual access for flow visualization and PIV capture. The slice comprises two fins and the air side is bounded by two isolating boards, forming three air channels. The power supply per unit depth was set to two different values, 2600 W/m and 3862 W/m. The second power corresponds to design operating conditions while the first (lower) power was chosen to observe the sensibility to power variations.

We present firstly a series of tests aimed to verify the satisfactory behavior of the experimental device. Then we present measurements of the heating transient and finally the steady state operation of the device. The experimental results are in good agreement with the steady state numerical solutions of [24] and [31], showing a stratified temperature distribution and a similar flow pattern in the studied region. We also performed preliminary numerical simulations using a 3D model of the slice used in the experiment. Based on the experimental results we decided not to introduce a turbulence model. The results of the numerical simulation are compared with the experimental measurements.

2. Experimental setup and measurement method

The Experimental Device (ED) was build in order to simulate a representative section of an ONAN (Oil Natural - Air Natural) 1000 KVA distribution transformer encompassing two fins. In the ED the heating by cooper losses in the transformer winding are simulated by an electrical heating element. A double glass window allows visual access for flow visualization and PIV capture. To achieve thermal similarity on the air natural convection side, the two fins were shielded with polystyrene foam boards, forming three air channels as sketched in Fig. 1 (Top view). This figure also shows the device dimensions and the reference coordinate system. The heating element consists of an aluminum structure as detailed in Fig. 1 (b). This structure was built with seven aluminum vertical plates 0.365 m high. These plates were connected through 12 lateral spacers and 6 central spacers that help uniformizing the temperature while keeping a rigid structure. The separation between the plates is about 8 mm and the free flow area is about 23 cm^2. Three Watlow FIREROD cartridge electrical heaters, with a diameter of 6.5 mm and a heating length of 50 mm each, were inserted perpendicular to these walls. These heaters were uniformly distributed along the vertical and in a good thermal contact with the aluminum plates. The seven aluminum plates and the spacers that conform the heating element achieve a satisfactory temperature uniformity given the high conductivity of aluminum as compared to the working fluid (coolant oil). The power was supplied to the heaters by means of a variable auto transformer.

According to data provided by Tubos Trans Electric S.A. from dissipation measurements of a transformer in no-load operation, power loss in the core accounts for 1740 W while the copper losses at full-load

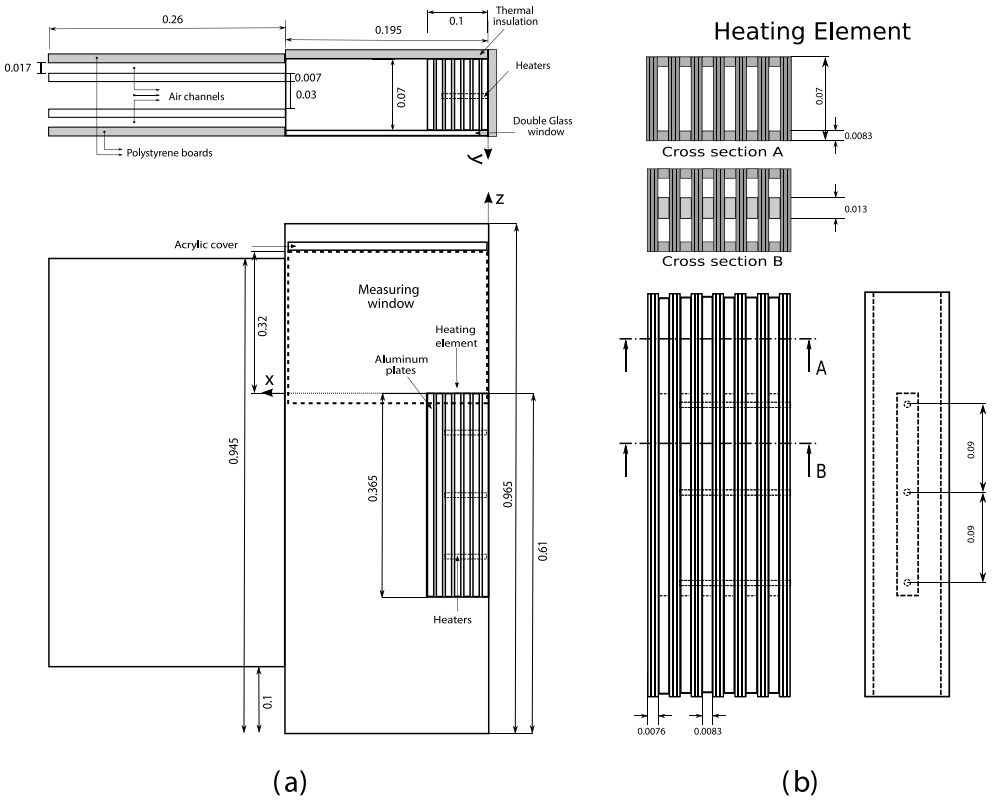

Fig. 1. Schematic of the experimental device. (a) (Bottom) Cavity front view, (Top) Cavity top view. (b) Heating element structure.

operation account for 10816 W. Core losses account for 20% of the losses, here we will focus on copper losses that account for 80% of the total power loss.

The test section comprises two fins of a total number of 80 and therefore we have taken a heating power of $P2 = 270$ W. Two reference powers were selected in the experiment: $P1 = 182$ W and $P2 = 270$ W in order to observe if there is a significant variation of the flow pattern as a function of the power input. These power values correspond to 2600 W/m and 3862 W/m power per unit depth respectively.

We differentiate two regions in the studied geometry: the tank region, where the heating of the oil takes place, and the cooling zone corresponding to the fins. The tank is open at the top to allow for easy access, oil manipulation and cleaning. The cavity is completely filled with mineral oil YPF64. The physical properties of this mineral oil were provided by Tubos Trans Electric S.A. and they are detailed in Table 1.

Once the ED is filled with oil, a floating acrylic cover is introduced. This cover supplies a non-slip boundary condition while allowing for volumetric expansion of the oil.

Five K type thermocouples were located at different points of interest in the device, as shown in Fig. 2 (a). Three of them, $T0$, $T3$ and $T4$, were inserted inside the cavity. $T0$ and $T3$ measure the oil temperature while $T4$ is used to obtain the temperature of the heating element. $T1$ and $T2$ measure the external surface temperatures at different points of the fin. The diameter of thermocouples are 1 mm for T0, 0.5 mm for T3, 0.7 mm for T1 and T2, and 0.8 mm for T4. The positions of the thermocouples are indicated in Fig. 2 (a). The thermocouple in position $T3'$ is a fast response thermocouple used to obtain the power spectrum of the temperature fluctuations.

Table 1
Fluid properties of the YPF64 oil.

Physical property		Value
Density (kg/m^3)	ρ	880
Thermal conductivity (W/(m K))	k	0.126
Specific Heat (J/(kg K))	C_p	1860
Thermal diffusivity (m^2/s)	α	7.7×10^{-8}
Thermal expansion coefficient (K^{-1})	β	0.00075

Temperature measurements were taken by a National Instruments NI 9219 universal analog input module connected to a PC. Additionally, a Fluke Ti100 thermal imaging camera was used to obtain temperature fields from the fin walls. The fin surfaces of the experimental device were painted matt black to allow more accurate optical temperature measurements.

In the real transformer, except for the first and last fins of a row, fins are sided by other fins at the same temperature, therefore there is no lateral radiation heat exchange. Heat is convected by the air that circulates between the fins and by radiation heat transfer to the surroundings. Ideally we would like to have a boundary condition of symmetry at half the air channel width from the external fins. This is not possible in an experimental device, we decided in turn to generate air gaps parallel to the external walls of the fins but to avoid radiation heat transfer. This was achieved by shielding the fins aluminized polystyrene foam boards but allowing a channel for the air to flow (see Fig. 1 (a: top view)), thus retaining air natural convection conditions. The separation between the fins and the polystyrene board walls was adjusted in order to obtain the same temperatures on the inner and outer walls of the fin. Best results were obtained for a separation of 1.7 cm and this separation was used for all the measurements of the present work. This translation symmetry approach has been verified by using thermal images of the experimental device, taken once the steady state was achieved, along with thermocouple measurements on the fin surfaces. The temperature fields obtained from the thermal camera, for both reference input powers are shown in Fig. 3. Figures A and C show the thermographies of the front surfaces of the fin. One of the polystyrene boards was momentarily removed for that purpose. Figures B and D correspond to thermal images taken on the front of the air channels. It was verified that the temperatures of the inner and outer

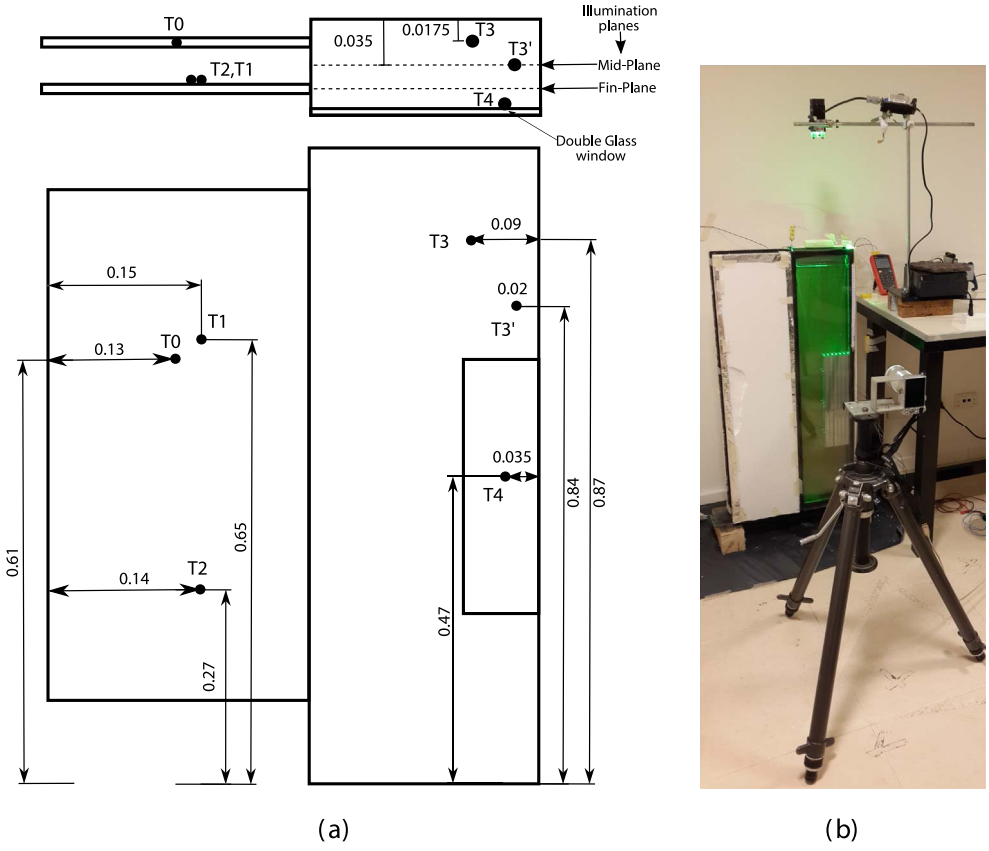

Fig. 2. (a) Thermocouple positions and illumination planes (Top) Top view, (bottom) front view. (b) Experimental array and PIV setup.

walls of the fins were equal within 2 °C.

Steady state was determined based on the settling times obtained from the evolution of the temperature data from thermocouples T0 to T3. To achieve a variation of less than 0.5 °C/h a continuous operation of approximately 12 h was necessary.

We used planar Particle Image Velocimetry (PIV) to obtain the velocity fields. We took advantage of the low velocities to be measured, approximately $\sim 10^{-2}$m/s, and designed an inexpensive PIV setup as shown in 2 (b). The images where captured by means of a Nikon 1 J5 digital camera, capturing 20 frames per second at a resolution of 20 Mpixel. For each flow field snapshot a burst of 20 consecutive frames were acquired and processed, obtaining 19 velocity fields, which allowed reducing uncertainty. In this setup the illumination plane was generated by a continuous green laser with a nominal power of 400 mW and a wave length of 532 nm, and a Powell cylindrical lens with a fan angle of 30° to expand the laser. This plane was alternatively placed at

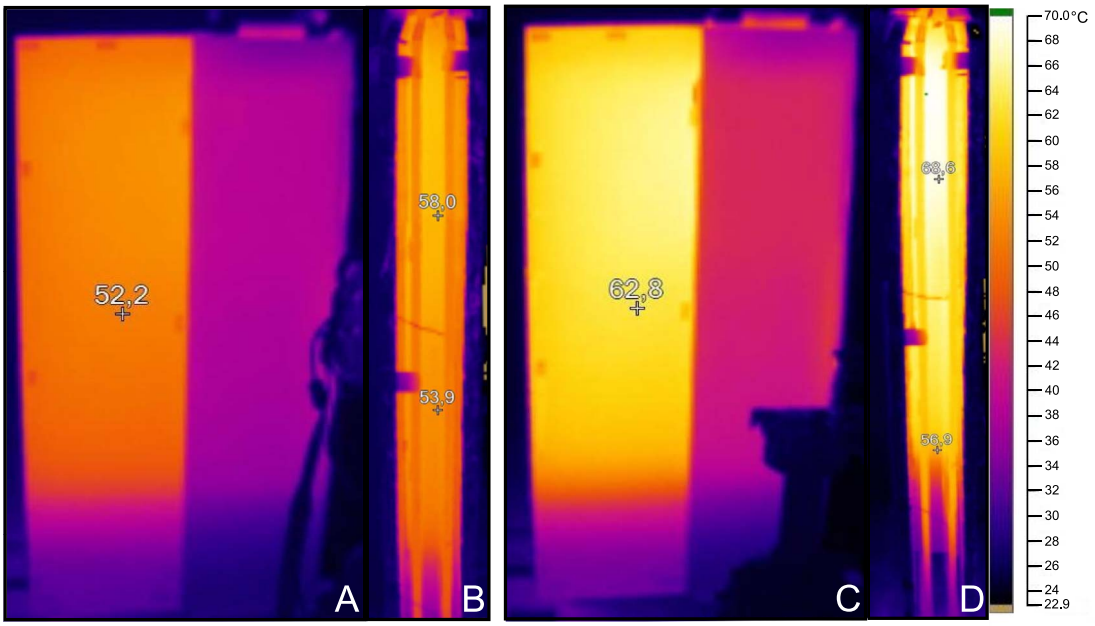

Fig. 3. Temperature fields at steady state. A,B: Power 182W. C,D: Power 270W.

two different offsets from the double glass window at $y = 0.0$ m (mid-plane) and at $y = 0.0175$ m (fin-plane) as shown in Fig. 2 (a) (Top view).

SPHERICEL® hollow glass particles 10 μm in diameter, with a density of 1.01 g/cm^3, were used as flow tracers. When this particles are illuminated the scattered light is recorded by the digital camera focusing on the laser illumination plane (see Fig. 2 (b)) in the measuring window (see Fig. 1 (a) Front view). We decided to limit the flow field measurements to the upper region of the test section, which is the area where the strongest convective flow takes place.

The PIV processing was performed by using the PIV ImageJ plugin [32] of the open source software ImageJ (http://rsb.info.nih.gov/ij). This plugin performs the cross correlation between consecutive pair of images. The correlation is calculated by dividing the image into interrogation windows. The criteria that we used to determine the size of these interrogation windows (d_I) is given by $d_I > 4d_{max}$ and $N_I > 10 - 20$, being d_{max} the maximum displacement of the particles and N_I is the image density, i.e. the number of particles within the interrogation window [33]. In present work, a $N_I \sim 328$ was achieved in an interrogation window of side 128 pixels. The particle diameter in the images varies approximately between 4 and 7 pixels.

We analyzed three possible error sources for the velocity field: image calibration error, image distortion and pixel binning. The camera we used in the present study is a color camera, which uses a Bayer filter array to produce the RGB color fields. As a result the most significant error source is pixel binning which arises from the interpolation of the camera Bayer filter array. An estimation of the error in the particle center location is 0.5 pixel which translates to an estimated velocity error of 0.6 mm/s.

3. Experimental results

3.1. Fluttering periodicity and sampling period

During the preliminary measurements it was observed that the rising oil plume at the outlet of the heating element presents oscillations in the form of fluttering. It was considered necessary to measure the periodicity of these oscillations in order to estimate the measurement time necessary to obtain satisfactory averaging of the velocity field.

Since the plume fluttering generates temperature fluctuations, we measured the instantaneous temperature at a point where significant plume oscillations were observed and we obtained the power spectrum estimate from this signal. The chosen position is marked as $T3'$ in Fig. 2 (a). Temperature measurements were taken after steady state operation was achieved at the power input of 270.4 W. The instantaneous temperature was recorded every 1.682 s during a total period time of 17 h.

It is worth mentioning that during this period the temperature signal presents drifts and fluctuations that exceed the fluid dynamic phenomenon, in particular ambient temperature variations. These small temperature drifts introduce low frequency components in the power spectrum of the temperature measurement but are unrelated to flow fluctuations. Ambient temperature drifts are small and extremely slow, therefore temperature gradients stay approximately constant as shown in the next section. As a result the effect on the velocity field is negligible. The power spectrum estimate is presented in Fig. 4 and shows a clear peak at a frequency of approximately 10^{-2} Hz, i.e. a period of 100 s. In the velocity field measurements, we want to be able to average the velocity fluctuations caused by the fluttering of this plume. We have therefore taken between 20 and 25 velocity field measurements during a total time span of 1000s. These measurements were then used to produce an ensemble average and to calculate the velocity fluctuation magnitudes. The fluttering of the plume introduce an additional error source in the mean velocity estimation due to the limited number of measurements that were used in the ensemble average. The maximum error is approximately 1.5 mm/s and is limited to the area affected by the plume.

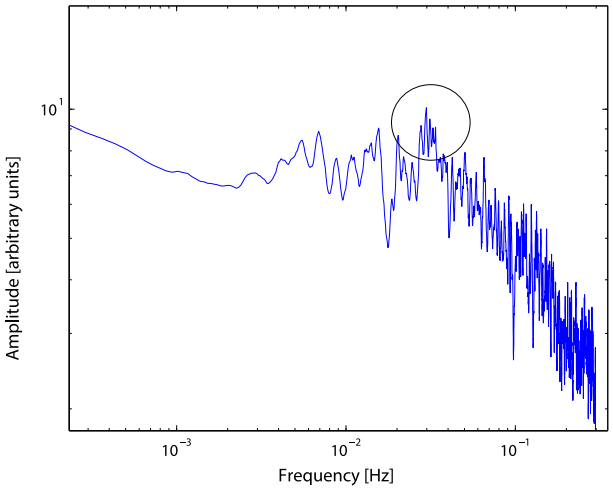

Fig. 4. Power spectrum estimate from the temperature measurements at the input power of 270 W.

3.2. Temperature evolution and heat transfer quantities

In order to determine the time required to achieve the steady state, the time evolution of temperature was measured at points of interest (see Fig. 2 (a)). The ambient temperature (Ta) was also measured by means of a UT322 thermometer. Temperature measurements for the two power inputs selected, are shown in Fig. 5. The asymptotic values obtained at steady state for each measurement point in the two cases are registered in Table 2.

It can be seen from Fig. 5 that the device takes approximately 700 min to achieve the steady state at a power input of 270 W while at the power input of 182 W, it takes about 500 min. In this figure the points where the 1000 s image acquisition periods begin are also indicated. These measurements are used to obtain the ensemble averaged velocity fields during the heating process.

Based on the electrical-thermal analogy, a thermal time constant can be defined as follows:

$$\tau_{th} = R_{th} C_{th} \tag{1}$$

where τ_{th} is the thermal time constant in minutes, R_{th} is the thermal resistance, and C_{th} is the thermal capacitance [34]. Based on (1), we estimated the thermal time constant of the heating element (τ_{HE}), as:

$$\tau_{HE} = \frac{m_{HE} c_{Al} (T_{HE} - T_{oil})}{q_{HE}} \tag{2}$$

where m_{HE} is the weight of the heating element, c_{Al} is the specific heat capacity of heating element material (aluminum), q_{HE} is the input power supplied to the heating element, T_{HE} is the temperature in the heating element and T_{oil} is the oil temperature. The weight of the heating element was estimated to be 4.9 kg. Considering the experimental temperature values of Table 2, where $T_{HE} = T4$ and $T_{oil} = (T3 + T2)/2$, we obtain $\tau_{HE} \sim 4$ min for $q_{HE} = 182$ W and $\tau_{HE} \sim 3$ min for $q_{HE} = 270$ W. Based on the temperature evolution shown in Fig. 5, we determined the thermal time constant of the ED as the time where the temperature reach the 63% of its asymptotic value. The time constants obtained were $\tau_{th,ED} = 46.8 \pm 1.2$ min for the input power P1 and $\tau_{th,ED} = 53 \pm 3$ min for P2. Since the thermal time constants of the heating element are one order of magnitude lower than the ED thermal constants, we can conclude that the dynamics of the heating element does not affect the dynamics of the whole system.

The thermal resistance of the ED is calculated as $R_{th,ED} = \Delta T_h / q_{HE}$, where ΔT_h is the temperature difference $T4 - Ta$ at the input power q_{HE}. In addition, we defined the heat transfer conductance per unit depth as $C' = q'_{HE}/(T4 - Ta)$, where q'_{HE} is the input power per unit depth $q'_{HE} = q_{HE}/\varepsilon$, being ε the depth of the considered section. In

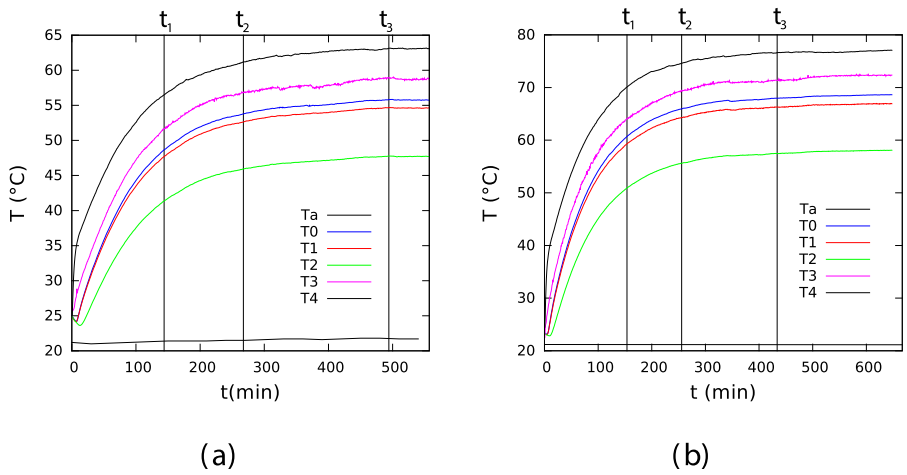

Fig. 5. Temperature evolution to steady state (a) 182 W, (b) 270 W. Ta state for ambient temperature while T0 to T4 are taken at positions specified in Fig. 2.

Table 3 we have summarized the characteristics times and the heat transfer quantities obtained by using the temperature experimental results and the equations mentioned above.

3.3. Velocity fields

Velocity fields measured at the times shown in Fig. 5, i.e. during the transient heating, for the two powers of interest can be seen in Fig. 6. Fields (a), (b) and (c) of this figure correspond to the power of 182 W while fields (d), (e) and (f) correspond to the power of 270 W. These fields were measured at the cavity mid-plane.

It can be seen in both cases, that the highest velocity values and greatest flow pattern changes appear during the initial transient of the heating process. As time increases the steady state flow pattern is established and velocity magnitudes decrease. During the first stages of the transient the hot plume shows a very high upward velocity. Close to this plume a downward jet is generated (see Fig. 6 (a), (b) and (d)). As the process evolves the downward jet becomes weaker giving place to a horizontal jet (see Fig. 6 (c), (e) and (f)). This process can be observed in measurements taken at both heating powers. It should be noted here the duration of the heating transient is shorter in the case of the higher heating power and therefore the snapshots for that case correspond to later stages of the transient evolution.

The velocity fields obtained from the two measurement planes, once the ED has achieved the steady state, are shown in Fig. 7. The velocity fields at the left side from this figure were measured at the cavity mid-plane while the ones at right side correspond to the fin plane.

The velocity fields show a rising plume that arises from the heating element. This plume contracts rapidly after leaving the heater and attaches to the vertical wall that supports the heater on the right side of the measurement domain. The mid-plane measurements show on the left side a downward flow due to the presence of the left vertical wall, while the fin-plane measurements clearly show how the flow enters the fin. It can also be noted that higher velocities are only found close to the walls, while in the central zone, velocities are one order of magnitude lower. A similar behavior can be seen in the case of natural convection in a cubical cavity at high Rayleigh numbers in Ref. [19].

Velocity fields measured in the fin plane show a significant horizontal flow that arrives to the outlet of the heating element, from the fin. In this plane we can see that the rising plume is composed by the horizontal flow coming from the fin and the outlet flow that arises from the channels of the aluminum plates that conform the heating element. Similar flow characteristics have been predicted by the numerical models of [24] and [31] related to similar distribution transformers.

Table 3
Characteristics times and the heat transfer quantities.

Power input	τ_{HE} (min)	$\tau_{th,ED}$ (min)	$R_{th,ED}$ (K/W)	C' (W/(m K))
182 ± 4 W	3.9 ± 0.9	46.8 ± 1.2	0.23 ± 0.01	63 ± 5
270 ± 4 W	3.1 ± 0.8	53 ± 3	0.20 ± 0.01	70 ± 5

In order to obtain a quantitative measurement of the plume velocities, velocity profiles along horizontal lines were taken from each velocity field along z = 10 cm and z = 20 cm. For the reference coordinate system, see Fig. 1. These velocity profiles are presented in Fig. 8. On each graph of this figure, the velocity profiles obtained at the input powers P1 = 182 W and P2 = 270 W were compared. It can be seen that in most cases except (b) the highest velocities and rising plume width correspond to the case of P2. It is noteworthy that the profiles for both powers in (b) are very similar and even the maximum velocity for P1 is slightly higher than the maximum for P2. When comparing velocity fields in Fig. 7 (b) and (d), the high velocity spot above the heater in (b), appears to be a local effect that may be caused by the three-dimensional nature of the flow.

In both measurement planes it can be seen that a small portion of the rising flow is deflected to the upper right corner of the cavity, generating a recirculation on the right vertical wall. This process causes the detachment of the plume from the wall, generating oscillations in form of fluttering and consequently strong fluctuations in the velocity field. To obtain the velocity fluctuation magnitudes, the standard deviation was calculated using the relation (3),

$$std(x, z) = \sqrt{\frac{1}{N}\sum_{i}^{N}(u_i(x, z) - U(x, z))^2} \quad (3)$$

Table 2
Temperature asymptotic values obtained at steady state for each measurement point. Temperatures are expressed in °C.

Power input	T0	T1	T2	T3	T4	Ta
182 ± 4 W	55.7 ± 0.3	54.6 ± 0.2	47.7 ± 0.3	58.7 ± 0.8	63.0 ± 0.2	21.5 ± 0.8
270 ± 4 W	68.5 ± 0.8	66.8 ± 0.8	58.0 ± 0.7	72.2 ± 0.6	76.8 ± 0.5	21.7 ± 0.6

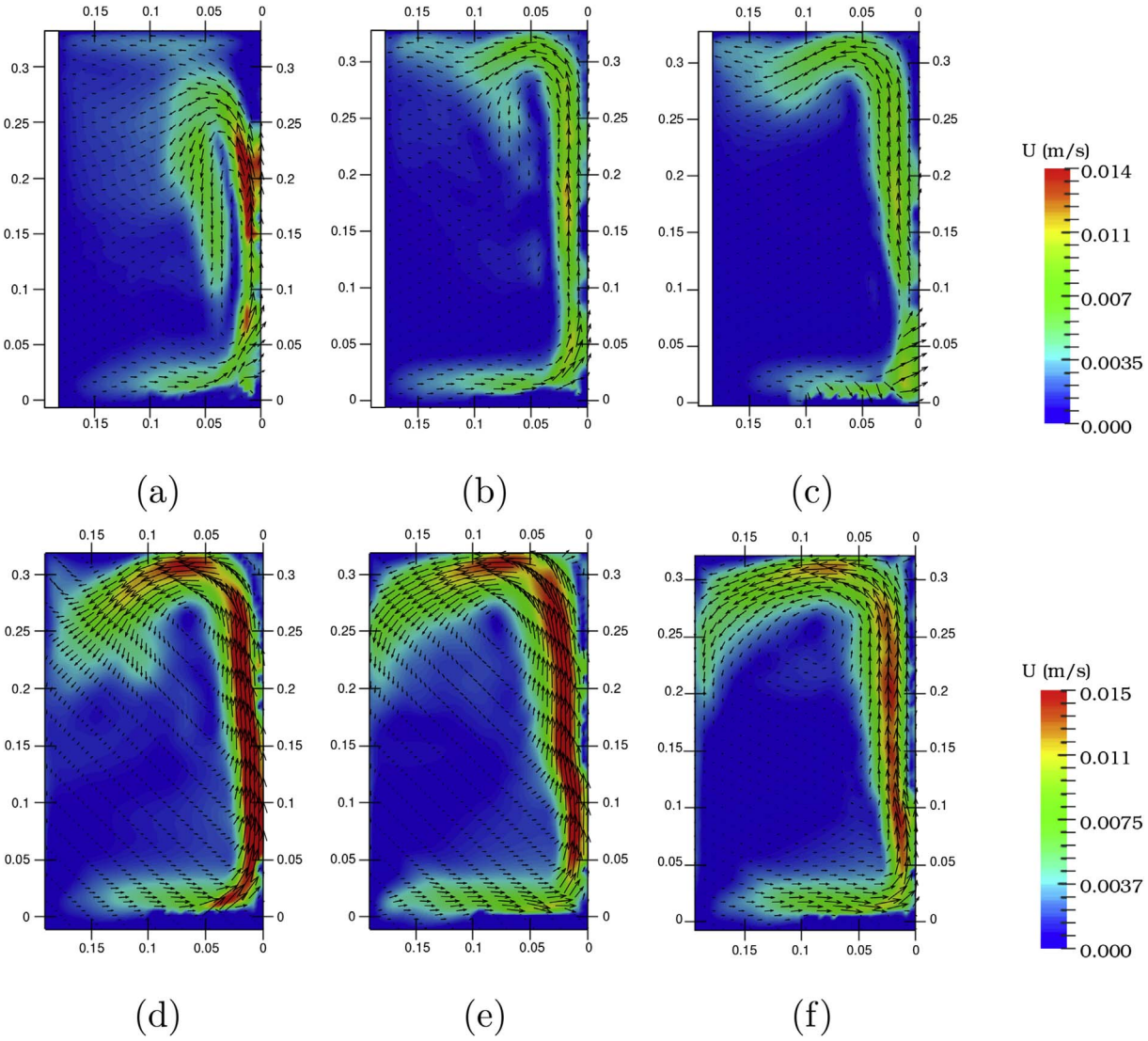

Fig. 6. Experimental velocity fields at cavity mid-plane during the transient heating for both power. 182 W: (a) t_1 = 144 min, (b) t_2 = 267 min, (c) t_3 = 494 min. 270 W:(d) t_1 = 154 min, (e) t_2 = 256 min, (f) t_3 = 434 min.

where $u_i(x, z)$ is the instantaneous velocity field, $U(x, z)$ is the mean velocity field, which is given as:

$$U(x, z) = \frac{1}{N}\sum_{i}^{N} u_i(x, z, t_i), \tag{4}$$

and N is the number of samples taken during the total time span of 1000 s. Fig. 9 shows the resulting velocity fluctuation fields for both measurement planes at the two input powers. The fields (a) and (b) from Fig. 9 correspond to the velocity fluctuation fields at cavity mid-plane, while (b) and (d) fields correspond to the fin-plane. It can be noticed that at the lower input power, i.e. 182 W, the velocity fluctuations are more significant near the right vertical wall extending to the upper right corner (see Fig. 9 (a) and (b)), while the flow is stable in the remaining cavity region. For the input power of 270 W, the most significant fluctuations also include the region near to the top wall (acrylic cover) of the cavity. In both cases, the horizontal flow coming from the fin to the outlet of the heating element do not present significant velocity fluctuations. The maximum velocity fluctuations are observed near to the right vertical wall corresponding to the region where the separation of the rising plume from the vertical wall occurs. It is notable that the higher velocity fluctuations occur at the cavity fin-plane. It is worth mentioning that in Fig. 9, we can observe small regions of low velocity fluctuations near the right vertical wall. We attributed this low turbulence to defects in the ED that obstruct the visibility and thus generate spurious low velocity regions.

It can be observed that the plume fluttering affects the direction in which the rising plume impacts the top wall generating velocity fluctuations near the upper fin inlet (see Fig. 9 (c) and (d)). In the case of the lowest input power, these lower order fluctuations are almost negligible (see Fig. 9 (a) and (b)). Also, even though the mean velocity fields in Fig. 7 (b) and (d) do not present plume separation from the right vertical wall, the fluctuation fields (see Fig. 9 (b) and (d)) show a strong fluttering in that region. This indicates that an intermittent separation occurs during the measurement time span.

4. Preliminary numerical results

Preliminary numerical results obtained in the framework of the work of [31] are presented in Fig. 10. The flow and temperature fields shown in this figure, correspond to slices of the numerical solution at the fin-plane (see Fig. 10 (a), (c)) and mid-plane (see Fig. 10 (b), (d)) of the 3D simulation domain. The numerical solution presented in this figure was averaged over a time span of 5000 s at steady state for the power input of 182 W. The simulation domain has the dimensions of the ED presented in Fig. 1. Only the volume occupied by the oil was

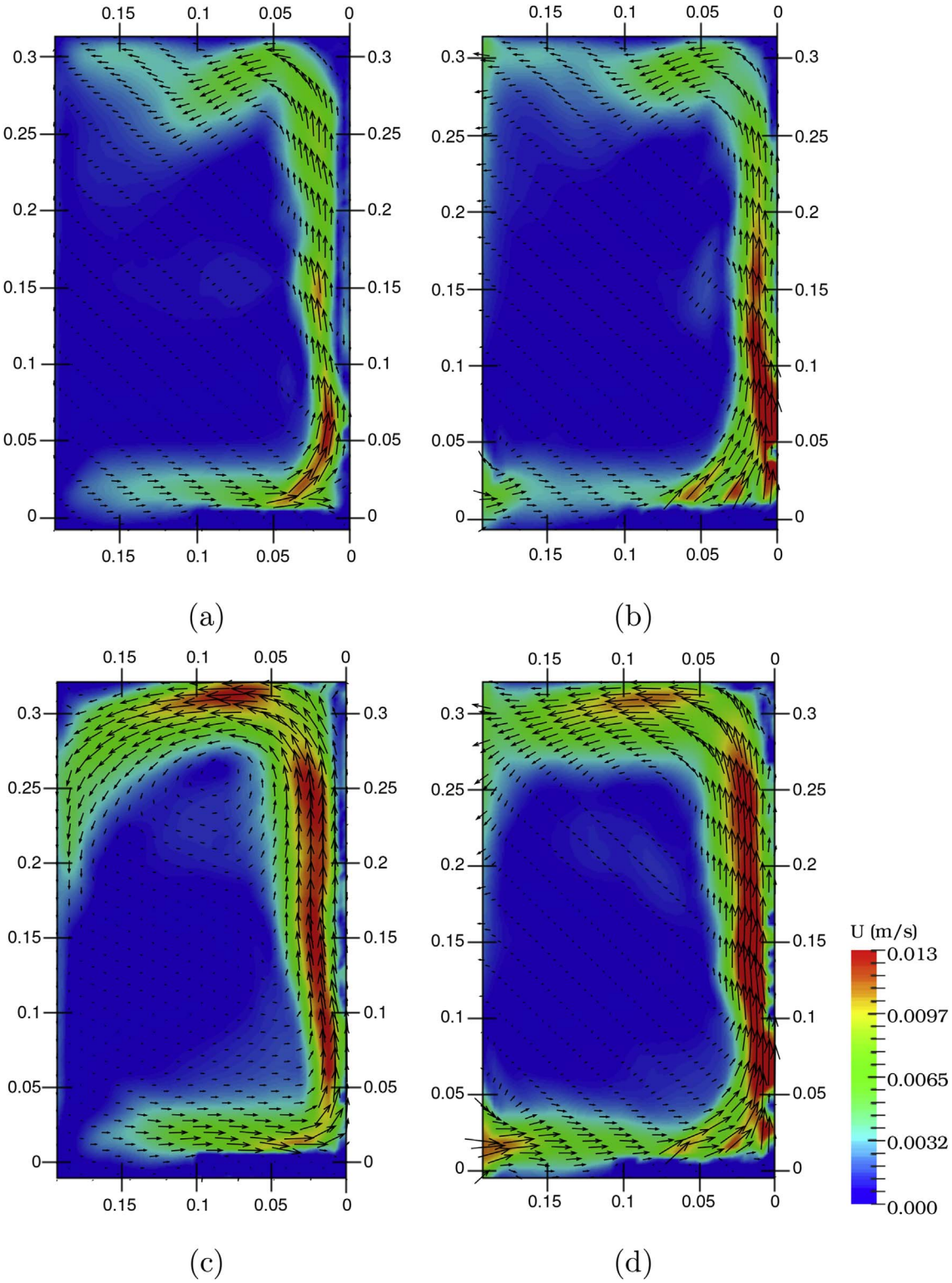

Fig. 7. Velocity fields at steady state. Power input of 182 W: (a) Mid-plane, (b) Fin-plane. Power input of 270 W: (c) Mid-plane, (d) Fin-plane.

simulated. We used a non uniform grid of 953856 tetrahedral elements and 173640 nodes. The minimal spatial discretization near the walls was $8{,}75 \times 10^{-4}$ m. Details of the grid and other numerical aspects can be found in Ref. [31].

The flow in the ED cavity is governed by the incompressible Navier-Stokes and energy equations, where the Boussinesq approximation is considered. The dimensional form of this equations can be expressed as

$$\rho_0[\partial_t u + (u\cdot\nabla)u] - \nabla\cdot[2\mu(T)\nabla^s u] + \nabla p = f, \tag{5}$$

$$\nabla\cdot u = 0, \tag{6}$$

$$\rho_0 Cp[\partial_t T + (u\cdot\nabla)T] - k\nabla^2 T = S, \tag{7}$$

in Ω, $t \in (0, T)$ where u is the velocity vector with components u_x, u_y and u_z. $f = \rho_0 g[1 - \beta(T - T_0)] - \rho_0 C_f u$, where the first term is the buoyancy force, being ρ_0 the oil density at the temperature T_0. The

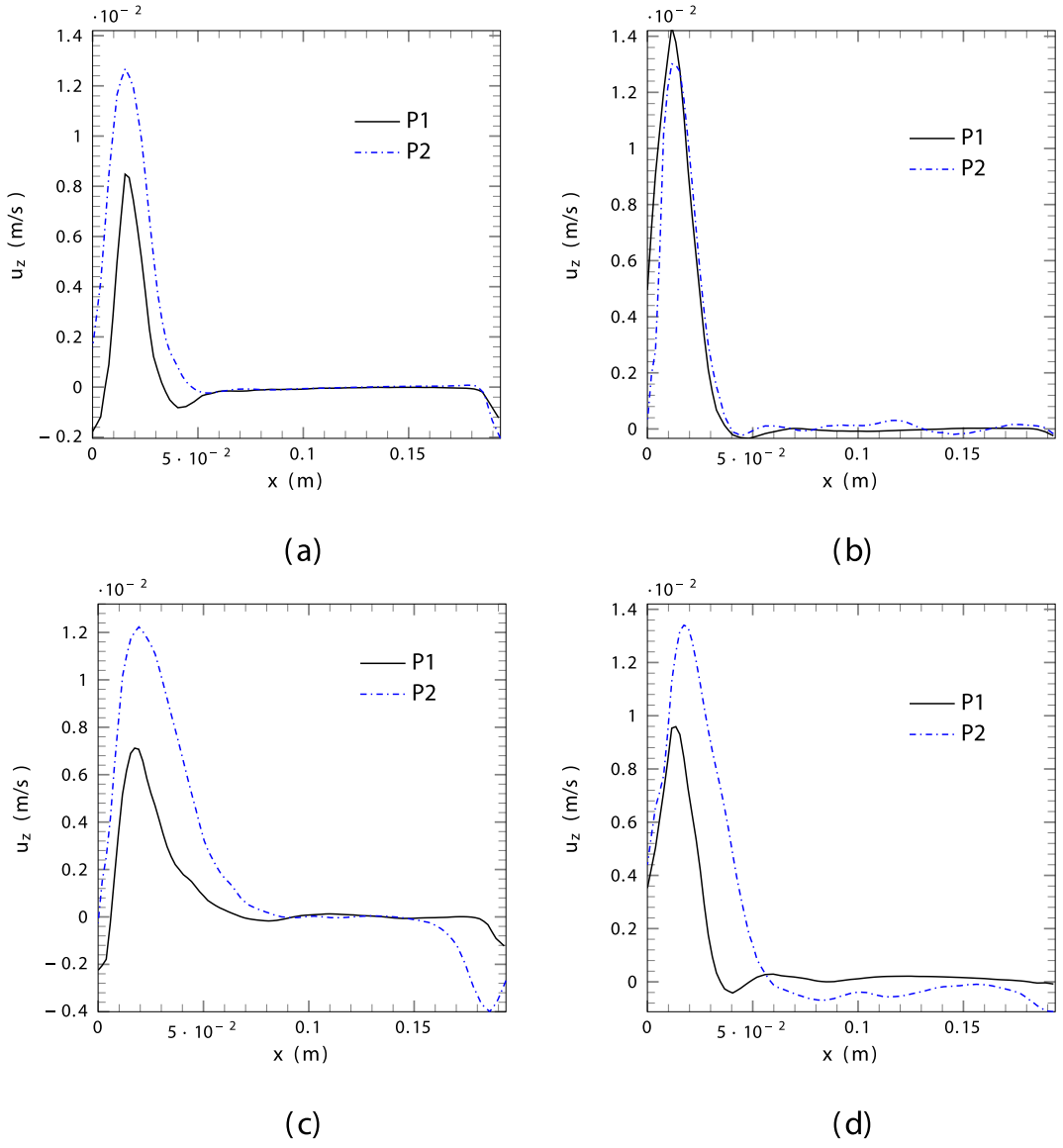

Fig. 8. Experimental velocity profiles at different heights (a), (b): z = 0.1 m (a) Mid-plane, (b) fin-plane. (c), (d): z = 0.2 m (c) Mid-plane, (d) fin-plane.

buoyancy force is written in this form to avoid the density evaluation at the local temperature. The second term is the Darcy's term used to model the heating element of the ED, being C_f a friction coefficient. $\nabla^s u = \frac{1}{2}[(\nabla u) + (\nabla u)^{\mathbf{T}}]$ is the symmetric gradient operator. Ω is the n -dimensional domain where the problem will be solved in the time interval $(0, T)$. μ is the oil viscosity which is dependent of the temperature T. The function $\mu(T)$ can be found in Ref. [19]. k and Cp are the thermal conductivity and the specific heat respectively of the working fluid. The physical properties of the mineral oil are detailed in Table 1. equations (5)–(7) have been solved by the Finite Element Method by using a stabilizing technique as is detailed in Refs. [19,31]. Based on the experimental results we decided not to introduce a turbulence model. We used no-slip boundary conditions for velocity, i.e. $u_x = u_y = u_z = 0$ at all walls. For the energy equation, the insulated walls have null Neumman boundary conditions $\frac{\partial T}{\partial \hat{n}} = 0$, while the remaining walls have convection boundary conditions: $k\frac{\partial T}{\partial \hat{n}} = \overline{h}(T_s - T_a)$. These conditions depend of the surface temperature T_s of the cavity walls and the convection coefficient $\overline{h}$. These convection coefficients were considered constants on each wall and they were estimated by using convective correlations from bibliography [34]. The power of the heating element was introduced in the model as a volumetric heat source (S in eq. (7)) acting in the heating element region. The preliminary results presented in Fig. 10 were obtained at the input power of 182W. It is worth noting that the thermal boundary conditions used in this simulation differ from the thermal experimental conditions in present study. In the simulation, one of the external walls of the one fin was thermally insulated while the remaining fin walls had convection boundary conditions with a constant convection coefficient. Despite these differences, both numerical and experimental flow fields are in good agreement.

5. Conclusions

In this work we present an experimental study of the flow and heat transfer in a test section representing a slice of an ONAN distribution transformer. We obtained the flow field in the upper region of the test section for two different heating powers including snapshots of the flow evolution during the initial transient. The overall heat transfer was also measured.

We designed the experimental setup to achieve translation symmetry in the thermal boundary conditions. The symmetry was verified by means of a thermal camera and thermocouple measurements, achieving temperature symmetry within 2 °C. The power supply per

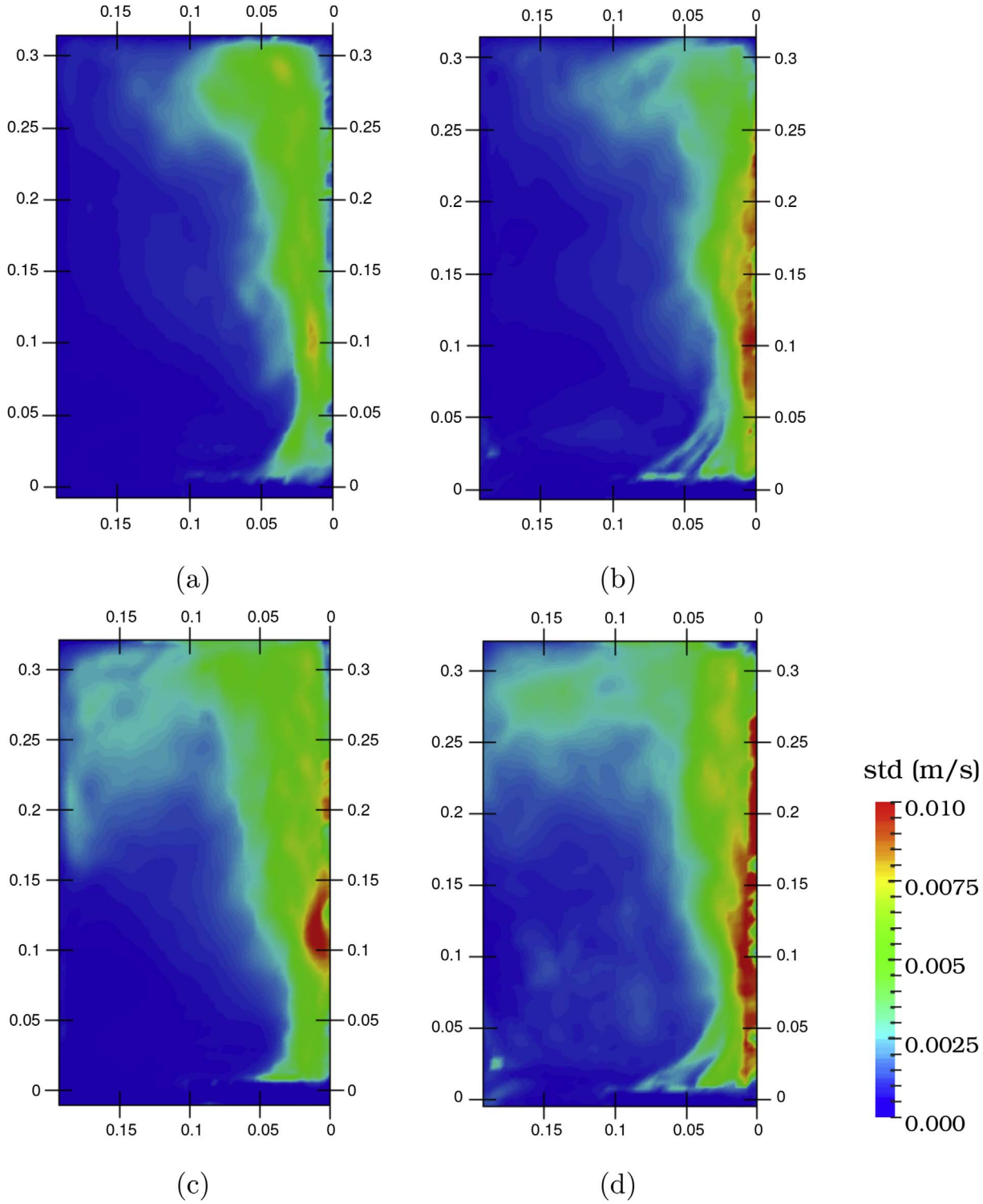

Fig. 9. Standard deviation of the velocity fields during the measurements at steady state. (left) Mid-plane, (right) Fin-plane. (a) and (b): power input of 182 W, (c) and (d): power input of 270 W.

unit depth was set to two different values, 3862 W/m and 2600 W/m. The first value agrees with the power used in a commercial distribution transformer (Tubos Trans Electric S.A. 1000KVA Standard Distribution Transformer), while the second value was adopted to verify the scalability of the results.

For the velocity measurements we took advantage of the low velocities involved and designed an inexpensive PIV setup. This PIV setup and methodology proved to be very satisfactory for the present flow characteristics. We decided to limit the flow field measurements to the upper region of the test section, which is the area where the highest flow takes place.

The measurement results show the flow pattern is characterized by the presence of a rising oil plume generated in the heating element. This plume contracts rapidly after leaving the heater and attaches to the vertical wall that supports the heater. As the plume rises it detaches from the wall and presents strong oscillations in form of fluttering,

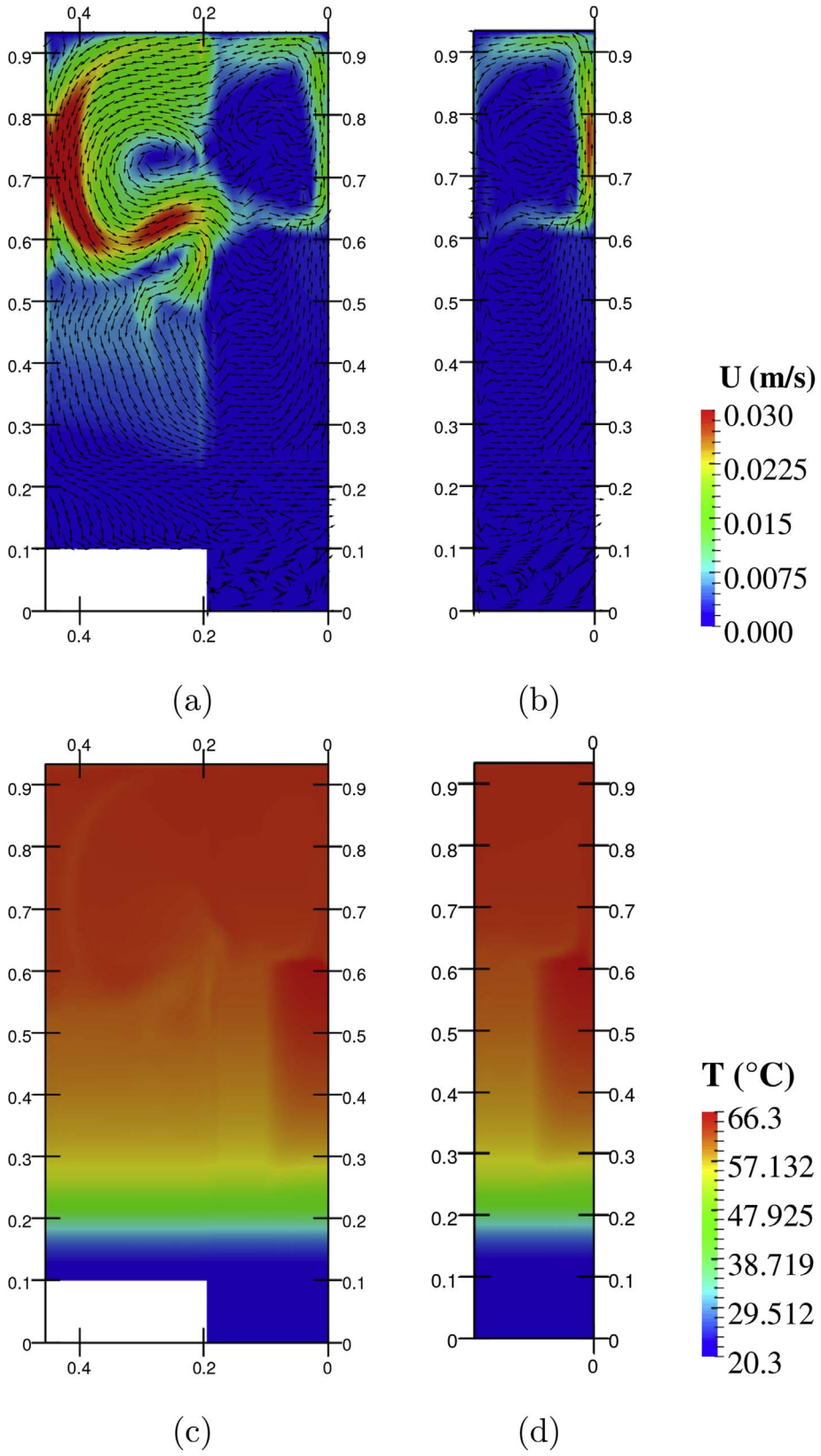

Fig. 10. Velocity (a,b) and temperature (c,d) fields obtained from preliminary numerical simulations of [31] at a power of 182W. (a) Fin-plane, (b) Mid-plane. (c) Fin-plane, (d) Mid-plane.

generating strong fluctuations in the velocity field. The most significant velocity fluctuations are found in regions affected by the rising plume, i.e. near the left vertical and top walls. The remaining regions of the test section showed very low velocity fluctuations. This may be due to stratification, acting as a stabilizing mechanism. This is also apparent from the temperature measurements, which show a stratified thermal distribution. We have also verified that the thermal and velocity fields obtained in present work are in good agreement with the predictions of

the numerical models of [24,31]. Some preliminary numerical simulation results are presented showing also good agreement with the experimental results.

The results obtained during the heating transient are of great interest as they show flow patterns that differ from those observed during steady state operation. Also the device shows a much larger heat transfer capability during the heating transient. The duration of the heating transient is long enough to be significant if compared to the daily variations of power loading. Measurements provide very valuable information about the duration and nature of the heating transient, but also show relevant features such as oscillations of the rising hot plume and the stabilization due to stratification. The present results may be useful to validate and improve numerical models and as reference to optimize the design of these devices.

The results obtained are in general in good agreement with previous results from numerical simulations. Even then, the detachment of the hot plume from the vertical wall as well as the fluttering of the rising plume were not previously reported. These features are not significant in terms of heat transfer performance but give important information on the sort of turbulent mixing to be expected.

Finally the transient evolution was measured and the thermal characteristic time of the system was estimated. It was found that the convection during the start-up transient is significantly stronger than during steady state operation.

Acknowledgment

We are grateful to Laboratorio de Ingeniería, Centro Atómico Bariloche, where the experiments were performed. We acknowledge financial support from ANPCyT (PICT-2016-0441), CONICET, CNEA and UNCuyo (PIB C026). We also want to thank Raul Stuke from Taller de Gerencia de Investigación Aplicada, Centro Atómico Bariloche for manufacturing of the cavity used as ED.

References

[1] IRAM 2018:1995, Transformadores de potencia, ensayos de calentamiento, Standard, Instituto Argentino de Normalización y Certificación, 1995.
[2] IEC 354:1991, Loading Guide for Oil-Immersed Power Transformers, Standard, International Electrotechnical Commission, 1991.
[3] IEC 60076–7:2005, Loading Guide for Oil-Immersed Power Transformers, Standard, International Electrotechnical Commission, 2005.
[4] M. Taghikhani, G. A, Prediction of hottest spot temperature in power transformer windings with non-directed and directed oil-forced cooling, Int J Electr Power Energy Syst 31 (2009) 356–364.
[5] D. Susa, M. Lehtonen, H. Nordman, Dynamic thermal modeling of distribution transformers, IEEE Trans Power Deliv 20 (2005) 1919–1929.
[6] D. Susa, M. Lehtonen, Dynamic thermal modeling of power transformers: further development-part i, IEEE Trans Power Deliv 21 (2006) 1961–1970.
[7] D. Susa, M. Lehtonen, Dynamic thermal modeling of power transformers: further development-part ii, IEEE Trans Power Deliv 21 (2006) 1971–1980.
[8] E. Koufakis, C. Karagiannopoulos, P. Bourkas, Thermal coefficient measurements of the insulation in distribution transformers of a 20kv network, Measurement 41 (2008) 10–19.
[9] M. Wang, A.J. Vandermaar, K. Srivastava, Review of condition assessment of power transformers in service, IEEE Electr Insul Mag 18 (2002).
[10] E. Hajidavalloo, M. Mohamadianfard, Effect of sun radiation on the thermal behavior of distribution transformer, Appl Therm Eng 30 (2010) 1133–1139.
[11] H. Buchberg, I. Catton, D.K. Edwards, Natural convection in enclosed spaces:a review of application to solar energy collection, J Heat Tran 98 (1976) 182–188.
[12] L.A. Volpe, Modelado y simulación de flujos turbulentos en reactores de investigación, Tesis de Grado Instituto Balseiro, 2013.
[13] G. De Vahl Davis, Natural convection of air in a square cavity: a bench mark numerical solution vol. 3, (1983), pp. 249–264.
[14] J.M. Hyun, J.W. Lee, Numerical solutions for transient natural convection in a square cavity with different sidewall temperatures, Int J Heat Fluid Flow 10 (1989) 146–151.
[15] F. Arpino, N. Massarotti, A. Mauro, High Rayleigh number laminar-free convection in cavities: new benchmark solutions, Numer Heat Tran, Part B: Fundamentals 58 (2010) 73–97.
[16] O. Younis, J. Pallares, F.X. Grau, Numerical study of transient laminar natural convection cooling of high Prandtl number fluids in a cubical cavity: influence of the Prandtl number, Int J Appl Sci Eng Technol 1 (2007) 107–112.
[17] T. Yamasaki, J. Thomas, F. Irvine, Laminar free convection in a vertical tube with temperature-dependent viscosity, Int J Heat Mass Tran 27 (1984) 1613–1621.
[18] J.M. Hyun, J.W. Lee, Transient natural convection in a square cavity of a fluid with temperature-dependent viscosity, Int J Heat Fluid Flow 9 (1988) 278–285.
[19] P.A. Córdoba, N. Silin, E.A. Dari, Natural convection in a cubical cavity filled with a fluid showing temperature-dependent viscosity, Int J Therm Sci 98 (2015) 255–265.
[20] D.R. Chenoweth, S. Paolucci, Natural convection in a enclosed vertical air layer with large horizontal temperature differences, J Fluid Mech 169 (1986) 173–210.
[21] S. Paolucci, D.R. Chenoweth, Transition to chaos in a differentially heated vertical cavity, J Fluid Mech 201 (1989) 379–410.
[22] L.W. Pierce, An investigation of the thermal performance of an oil filled transformer winding, IEEE Trans Power Deliv 7 (1992) 1347–1358.
[23] P. Daponte, D. Grimaldi, D. Villaci, A neural diagnostic system for monitoring of transformer heating, Measurement 18 (1996) 35–46.
[24] J. Gastelurrutia, J.C. Ramos, G.S. Larraona, Numerical modelling of natural convection of oil inside distribution transformers, Appl Therm Eng 31 (2011) 493–505.
[25] V. Galdi, L. Ippolito, A. Piccolo, A. Vaccaro, Parameter identification of power transformers thermal model via genetic algorithms, Elec Power Syst Res 60 (2001) 107–113.
[26] N. El Wakil, N. Chereches, J. Padet, Numerical study of heat transfer and fluid flow in a power transformer, Int J Therm Sci 45 (2006) 615–626.
[27] F. Torriano, P. Picher, M. Chaaban, Numerical investigation of 3d flow and thermal effects in a disc-type transformer winding, Appl Therm Eng 40 (2012) 121–131.
[28] F. Torriano, M. Chaaban, P. Picher, Numerical study of parameters affecting the temperature distribution in a disc-type transformer winding, Appl Therm Eng 30 (2010) 2034–2044.
[29] J. Gastelurrutia, J.C. Ramos, A. Rivas, G.S. Larraona, J. Izagirre, L. del Río, Zonal thermal model of distribution transformer cooling, Appl Therm Eng 31 (2011) 4024–4035.
[30] M.A. Tsili, E.I. Amoiralis, A.G. Kladas, A.T. Souflaris, Power transformer thermal analysis by using an advanced coupled 3d heat transfer and fluid flow fem model, Int J Therm Sci 53 (2012) 188–201.
[31] P. Córdoba, Estudio Numérico y Experimental para la optimización Termo-Fluido-Dinámica de transformadores de distribución tipo ONAN, Ph.D. thesis (2016).
[32] Q. Tseng, E. Duchemin-Pelletier, A. Deshiere, M. Balland, H. Guillou, O. Filhol, et al., Spatial organization of the extracellular matrix regulates cellcell junction positioning, Proc Natl Acad Sci USA 109 (2011) 1506–1511.
[33] R. Goldstein, Fluid mechanics measurements, Taylor & Francis, 1996.
[34] F. Incropera, D. DeWitt, Fundamentals of heat and mass transfer, John Wiley & Sons, 1996.